









Brief Report

# A Bunch of YBCO Josephson Generators for the Analysis of Resonant Cold-Electron Bolometers

Leonid S. Revin <sup>1,2</sup>, Dmitry V. Masterov <sup>2</sup>, Alexey E. Parafin <sup>2</sup>, Sergey A. Pavlov <sup>2</sup>, Dmitry A. Pimanov <sup>1</sup>, Alexander V. Chiginev <sup>1,2</sup>, Anton V. Blagodatkin <sup>1,2</sup>, Igor V. Rakut' <sup>1,2</sup>, Evgenii V. Skorokhodov <sup>2</sup>, Anna V. Gordeeva <sup>1,2</sup> and Andrey L. Pankratov <sup>1,2,\*</sup>

<sup>1</sup> Superconducting Nanoelectronics Laboratory, Nizhny Novgorod State Technical University, n.a. R. E. Alekseev, GSP-41, Nizhny Novgorod 603950, Russia

<sup>2</sup> Institute for Physics of Microstructures of RAS, GSP-105, Nizhny Novgorod 603950, Russia

\* Correspondence: alp@ipmras.ru

**Abstract:** The resonant properties of Cold-Electron Bolometers (CEBs) located at a 0.3 K cryostat plate are measured using a 50  $\mu\text{m}$  long high-temperature  $\text{YBa}_2\text{Cu}_3\text{O}_{7-\delta}$  (YBCO) Josephson junction oscillator, placed on a 2.7 K plate of the same cryostat. For these purposes, a bunch of YBCO Josephson oscillators with various lengths of dipole antennas and overlapping generation bands has been developed and investigated in 50–500 GHz frequency range. Two setups of Josephson junction placement were compared, and as a result, various narrow-band receiving systems with CEBs have been measured, demonstrating the feasibility of the presented approach.

**Keywords:** high- $T_c$  Josephson junction; anisotropic grain-boundary; YBCO; cold-electron bolometer; resonant properties



**Citation:** Revin, L.S.; Masterov, D.V.; Parafin, A.E.; Pavlov, S.A.; Pimanov, D.A.; Chiginev, A.V.; Blagodatkin, A.V.; Rakut', I.V.; Skorokhodov, E.V.; Gordeeva, A.V.; et al. A Bunch of YBCO Josephson Generators for the Analysis of Resonant Cold-Electron Bolometers. *Appl. Sci.* **2022**, *12*, 11960. <https://doi.org/10.3390/app122311960>

Academic Editors: Matt Oehlschlaeger and Mona M. Hella

Received: 24 October 2022

Accepted: 21 November 2022

Published: 23 November 2022

**Publisher's Note:** MDPI stays neutral with regard to jurisdictional claims in published maps and institutional affiliations.



**Copyright:** © 2022 by the authors. Licensee MDPI, Basel, Switzerland. This article is an open access article distributed under the terms and conditions of the Creative Commons Attribution (CC BY) license (<https://creativecommons.org/licenses/by/4.0/>).

## 1. Introduction

An important task for the study of cryogenic narrow-band bolometric systems is to develop a broadband radiation source with the possibility of continuous frequency tuning in the selected frequency range from tens to hundreds of GHz. It is also desirable that the emitting system is located inside the cryostat to avoid reflections from screens and background illumination from open windows, as well as to decrease the internal noise of an oscillator due to the lower operating temperature. As sensitive receivers, we use Cold-Electron Bolometers (CEBs) [1,2] with direct electron cooling of the absorber, that demonstrate photon-noise limited operation [3–5] and can potentially reach single-photon level sensitivity in the cm wavelength range [6]. Earlier, it was reported on the frequency response measurements of CEBs performed using a mercury arc lamp source [7], broadband thermal sources [3–5,8], and external room temperature sources of THz range [9,10]. These solutions are not very suitable in the case of a study of resonant narrow-band structures in various frequency ranges. Therefore, we develop the concept of the source of the sub-THz frequency range based on a bunch of long  $\text{YBa}_2\text{Cu}_3\text{O}_{7-\delta}$  (YBCO) Josephson junctions (JJ).

High critical temperature YBCO bicrystal long Josephson junctions [11–17] and arrays [18,19] can be used for spectral calibration of sensitive low temperature receivers, such as semiconductor single-photon detectors [20], bolometers [21–24] or integrated superconducting heterodyne receivers [19,25]. Josephson YBCO generators are convenient to use for the mentioned goals since their working frequency is connected with the voltage by the Josephson relation and at the same time they have a broadband continuous frequency tuning in the THz range [23].

In this work, for broadband frequency tuning, we use the so-called “travelling wave” or “flux flow” regime that occurs in a long JJ [23]. If a JJ is rather long with length  $L \gg \lambda_J$ , where  $\lambda_J$  is the Josephson penetration depth, the train of Josephson vortices (fluxons)

is created due to the effect of the magnetic field and radiated at an output edge after propagation along the junction.

The aim of the current work is to compare two setups of Josephson junction placement and to test various narrow-band detecting systems with Cold-Electron Bolometers to demonstrate the feasibility of the suggested technique.

## 2. Experimental Setup

The used experimental setup consists of long YBCO Josephson junctions as tunable THz sources, bolometers with direct electron cooling of the absorber as sensitive receivers and various holders and horns, feeding the radiation from a source to a receiver.

In Figure 1, the photographs of YBCO JJs inside the modified dipole antennas are demonstrated. The distributed Josephson junctions on the basis of the  $\text{YBa}_2\text{Cu}_3\text{O}_{7-\delta}$  thin films were fabricated by the method of the preliminary topology mask [16,17] using magnetron sputtering on  $24^\circ$ [001]-tilt  $\text{Zr}_{1-x}\text{Y}_x\text{O}_2$  bicrystal substrate. This technology assumes the preliminary deposition of cerium dioxide ( $\text{CeO}_2$ ) on the heated  $\text{Zr}_{1-x}\text{Y}_x\text{O}_2$  (or any other suitable) substrate as a buffer layer. Due to the high temperature, this buffer  $\text{CeO}_2$  layer provides an epitaxially clean surface; thus, the further deposition of the YBCO layer will lead to a superconducting film. Using the photoresist mask, a structure of Josephson junctions with electrodes is formed, and the further deposition of thick  $\text{CeO}_2$  layer on a cold substrate leads to an amorphous layer. The sputtering of YBCO film is performed as the final stage of the fabrication process. In this case, the YBCO film, sputtered on the epitaxially clean surface, becomes superconducting, but on the amorphous  $\text{CeO}_2$  layer it becomes insulating. Since the deposited superconducting structures have rather small sizes, this method allows a small number of defects together with high electrophysical properties of the films [17]. The Josephson junctions' length was  $50\ \mu\text{m}$  (along the grain boundary) with  $0.3\ \mu\text{m}$  film thickness. At the temperature  $T = 5\ \text{K}$ , the achieved critical current density is  $370\ \text{kA}/\text{cm}^2$  and the  $I_c R_n$  product is  $1.54\ \text{mV}$ . The junctions are rather long, with lengths much larger than the Josephson penetration depth  $\lambda_J = 0.6\text{--}0.9\ \mu\text{m}$ . The oscillator chip is formed with six JJ structures placed inside the modified dipole antennas. Since the generation of each junction can be continuously tuned from  $0.05$  to  $2\ \text{THz}$  [21], its oscillation frequency is determined by the antenna band. The numbering of the structures on the substrate is shown in Figure 1a. The scanning electron microscope (SEM) image of a structure is presented in Figure 1b. Here, one can observe the YBCO film, deposited on the epitaxially clean  $\text{CeO}_2$  buffer layer on  $\text{Zr}_{1-x}\text{Y}_x\text{O}_2$  substrate (blue) and the walls (burgundy) of a thick amorphous  $\text{CeO}_2$  layer as a part of a preliminary mask layer.

To develop and study the oscillators based on high-temperature bicrystal Josephson junctions we have used Cold-Electron Bolometer (CEB) array with broadband antennas [23], that were developed in [5,10,26]. While these antennas receive signal at multiple harmonics as well [23], they may limit the band of YBCO oscillator antennas, which has been improved in comparison with [23]. The CEB represents double SIN (superconductor-insulator-normal metal) junctions  $\text{Al}/\text{Al}_2\text{O}_3/\text{Al-Fe}/\text{Al}_2\text{O}_3/\text{Al}$  with tiny normal metal absorber made of aluminum with  $1\ \text{nm}$  thin underlayer of Fe to suppress superconductivity, which also allows achieving deep electron cooling [27]. The considered receiving systems are single elements with double-folded slot antennas, connected by coplanar lines, as well as a 2-dimensional array of bow-tie antennas with CEBs. Both types of receiving systems allow achieving rather narrow bandwidths. Besides photon-noise level sensitivity [3–5] and cosmic rays immunity [28], one more advantage of the CEB is its tiny size of a few microns, which allows depositing bolometers inside the antenna slots or coplanar lines without any additional microwave lines. This allows to solve a problem of high signal losses in long microstrip lines at high frequencies [29] and greatly simplifies the design of arrays [5], allowing fabrication of resonant narrow-band systems with on-chip filters [30].

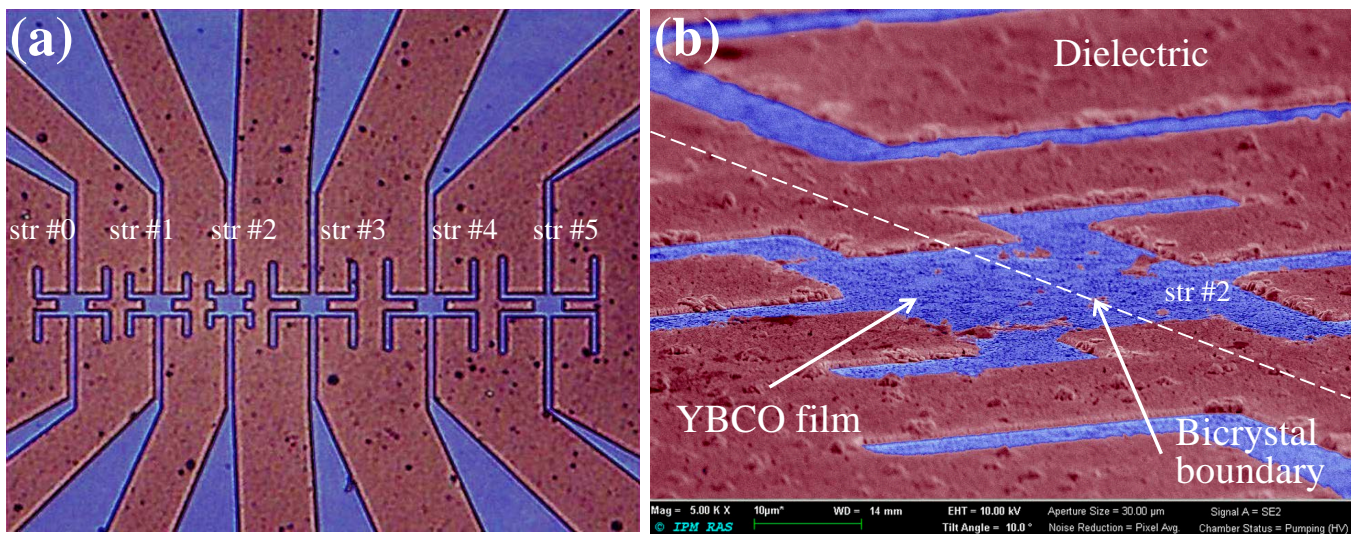


**Figure 1.** Photograph (a) and SEM image (b) of a sample with structures of YBCO JJ generators.

To obtain the highest signal-to-noise ratio of the receiving system, two schemes of the experimental setup inside a 300 mK closed-cycle Oxford  $^3\text{He}$  refrigerator were tested, see Figure 2. In both setups, the generator chip with JJs is attached to the sample holder with 4 mm hyperhemisphere silicon lens, placed at the 2.7 K plate of the refrigerator. Since the oscillators with their antennas are shifted together, even when the antennas are away from the centre of the lens, the corresponding beams are guided by the horns, so for all radiating structures, the signal reaches the used sensitive receiver and gives a response. The copper-wire coil is used for the control of the magnetic field, perpendicular to the Josephson junction boundary. A bolometer is placed on a 300 mK plate of the cryostat with a lens or a horn placed on the front or back side of the silicon substrate depending on the elaborated system. The receiver is covered by a copper shield to avoid radiation from other directions [4,5]. The first configuration (Figure 2a) assumes the maximum response of the detector, since the source of the sub-THz signal is as close as possible to the receiver: the distance between the bolometer and the generator is 3 cm. In this case, the generator is thermally coupled with a 2.7 K plate using a long brass rod. However, some overheating and out-of-band radiation of the Josephson source lead to an increase in the receiver noise. The second configuration (Figure 2b) assumes the location of the generator directly on the 2.7 K plate far from the receiver. At the same time, in order to collect the maximum part of the radiation and bring it to the bolometer, an oversized brass horn has been used. Thus, it is possible to more effectively cool the generators when a bias current is passed through them and to avoid the overheating of the receiving system by the out-of-band radiation. However, the level of the received signal turned out to be much lower than in the first case. The measurements have demonstrated that for the close location of the emitter, the response is 15 times greater than for the second setup. At the same time, the detector noise in the first case is 10 times larger. Thus, the signal-to-noise ratio for both configurations differs slightly. This provides flexibility in carrying out measurements of resonant bolometers. Each CEB structure is designed for different requirements of the power level of the incident signal. To prevent saturation of the bolometer due to too much power, we have the ability to move the generator closer or further from the receiver besides certain power tuning by changing the oscillation regime with the magnetic field from the phase rotation mode to the travelling wave regime [23]. Changing the Josephson junction bias current, we can record the bolometric response and the central radiation frequency. The bolometric response is defined as a voltage difference at a fixed bias current through the CEB with and without the JJ radiation. The voltage on the YBCO generator directly

determines the Josephson radiation frequency  $f = 2eV_{YBCO}/\hbar$ , where  $e$  is the elementary charge and  $\hbar$  is the Planck's constant.

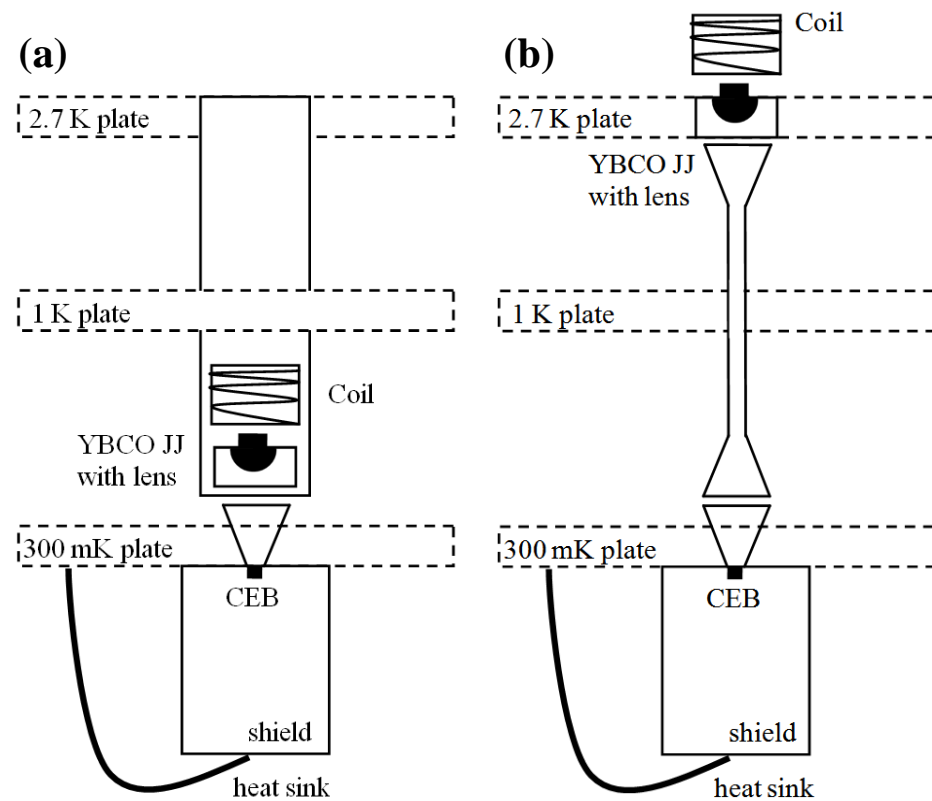


**Figure 2.** Schematic representation of two setups with closer (a) and remote (b) placement of YBCO Josephson generators for the study of the amplitude-frequency characteristics of bolometers.

### 3. Experimental Results

For preliminary measurements of the radiation bandwidths of YBCO oscillators a sample, representing array of broadband dipole antennas with CEBs [23] has been used. In Figure 3, the response versus frequency of the same CEB sample to radiation from different JJ structures is shown by solid curves. For comparison, dashed curves show the results of electromagnetic simulations for these structures. The positions of the main radiation maxima approximately coincide with theoretical expectations, while the widths of the maxima in the experiment are somewhat smaller and are restricted by the CEB antennas, since the bands of the modified dipole antennas, shown in Figure 1, are broader than the previous ones, used in [23]. In addition, half harmonics and doubled harmonics are visible on the measured amplitude-frequency characteristics (AFCs). The narrowing of resonant curves and the appearance of half harmonics can probably be explained by the fact that the modeling has not accounted for the possible back effect of resonant loading on the dynamics of an essentially nonlinear system, which is a long Josephson junction. The doubled harmonics have lower intensity than in the simulations. Perhaps this is due to the fact that at such high frequencies, the Josephson generation becomes weaker due to the effect of surface losses, increasing with frequency. The presence of other harmonics in the AFC of the generators makes it possible to use them more flexibly to analyze the resonant properties of bolometers. A total of 5 JJ structures were studied, only three of which are shown in Figure 3. In accordance with the designations of Figure 1, their main emission maxima are as follows: str#0—222 GHz, str#1—257 GHz, str#2—380 GHz, str#3—180 GHz, str#4—158 GHz. The advantage of using a bunch of JJ oscillators with different dipole antennas for various frequencies (compared to using a single oscillator with a broadband antenna) is due to the low impedance of such generators. It is known [11,31] that the

impedance of YBCO Josephson junctions is normally not larger than a few Ohms. In this case, unlike a broadband antenna with an impedance close to 50 Ohms, the dipole antenna can be modified to match the impedance of the single JJ.

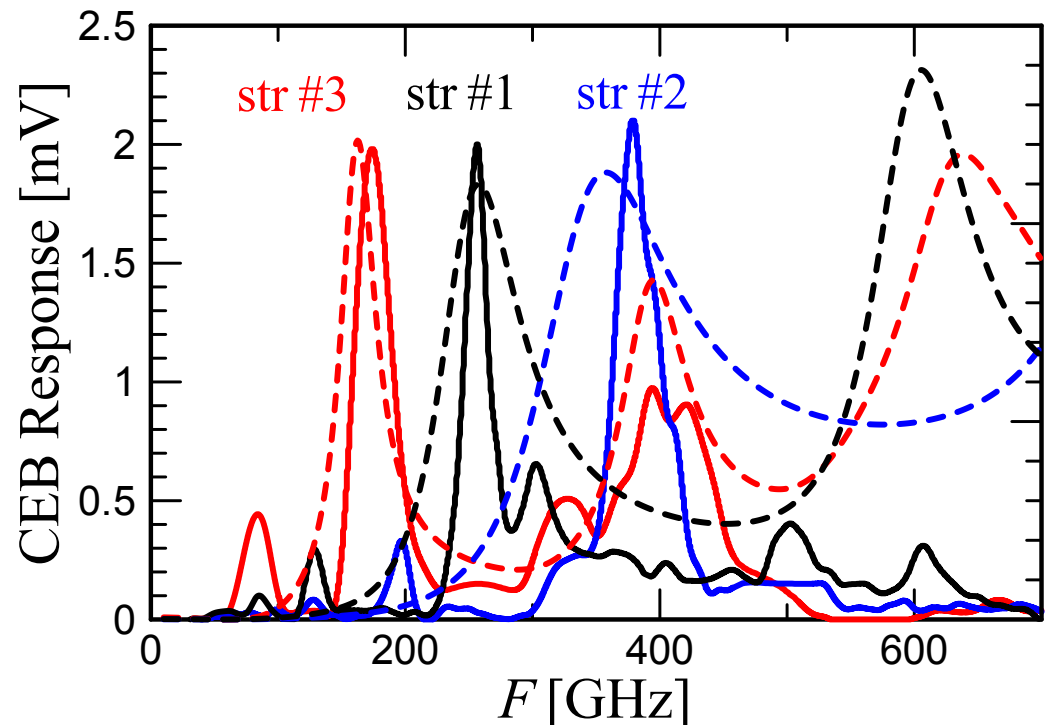


**Figure 3.** Amplitude-frequency response of a broadband bolometer to the radiation of three JJ generators. Solid curves—measurements, dotted curves—electro-magnetic modeling of JJ antennas. Structure notations correspond to Figure 1.

After characterizing the oscillators themselves, they have been used to study resonant systems based on Cold-Electron Bolometers, whose AFCs are narrower than that of the JJ oscillators. In Figure 4, the examples of the characteristics of three different receiving systems designed for different tasks in different frequency ranges are demonstrated. Due to the different response values of resonant bolometers, the figure shows the normalized characteristics for clarity.

The black curve corresponds to the frequency response of the seashell 75 GHz antenna with CEBs [30]. This antenna represents one polarization channel of the multichroic seashell antenna system with polarization resolution, proposed in [32]. The internal resonance is organized by a series resonance of the capacitance of the SIN tunnel junctions and  $\lambda/2$  slots for 75 and 105 GHz. For proper RF matching, slots and CEBs are connected by coplanar waveguides near the slot ends. Each CEB includes two SIN junctions with a nano-absorber. Such single element receiving system is intended for powers below 1 pW [4].

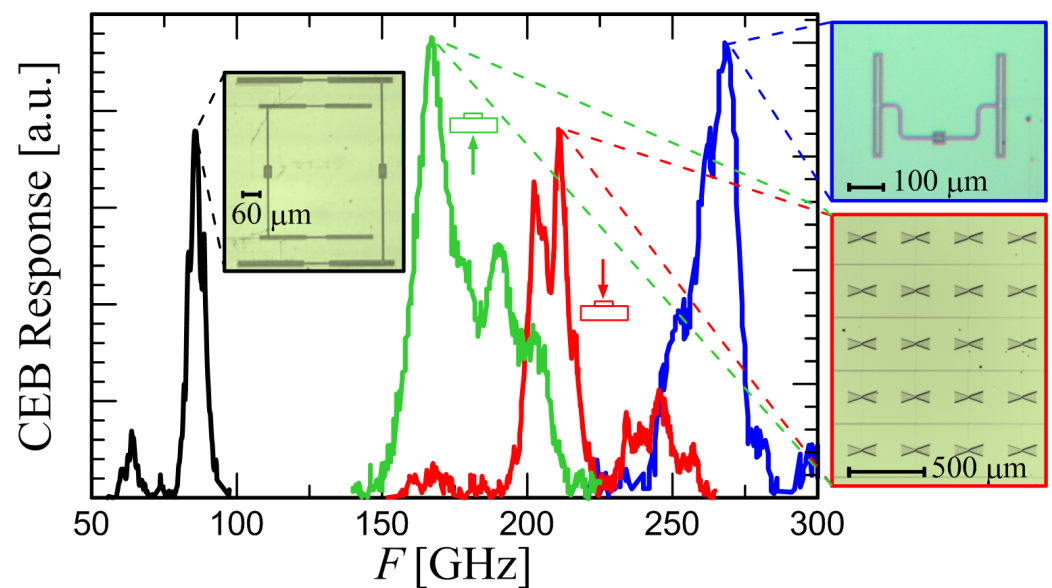


**Figure 4.** Frequency response of three resonant CEB structures, measured by YBCO Josephson generators. The photographs show the elemental structure of the studied samples.

The blue curve corresponds to the response of the single receiving cell based on a double-folded slot antenna with CEBs for the 220/240 GHz frequency range [24]. This system is a combination of the double-folded slot antennas designed to receive signals of various frequencies and is polarization sensitive. This antenna differs from the previous one by two things. First, the coplanar lines are connected in the middle of each slot for making the electromagnetic field distribution symmetric along the slot, and thus improving the radiation diagram of the antenna. Second, we use the central electrode in each slot for making narrower resonances of the receiving system. The coplanar line is also used to match the low impedance of the bolometers and the high impedance of the slot antenna. In addition, the length of the coplanar lines was adjusted to obtain the required operation frequency. Conductors are connected to the lumped capacitances, providing direct current or voltage bias of the CEB and connecting single antenna cells into a series or parallel array, respectively.

Different from the two above described systems, the next analyzed receiver represents many-absorber detector with multiple dipole type antennas, intended for LSPE mission [33] with tens pW power range. The simulation results for this system have been recently presented in [34], and here we demonstrate the first measurement results of the first fabricated sample for the 210 GHz frequency range. This sample has 44 bow-tie dipole antennas for 210 GHz frequency range. These dipoles are connected in parallel for DC to further use this array with the SQUID readout. The length of a single dipole is 185  $\mu\text{m}$ , the wide end of a dipole petal is 60  $\mu\text{m}$  and its narrow end, located near the Cold-Electron Bolometer connection to the antenna, is 10  $\mu\text{m}$ . Another difference of the current design with the previous samples is the use of SINS structures with Andreev contact instead of typical SINIS structures. Unlike two other structures, this system has been designed to receive the signal from the side of antenna layer. However, preliminarily it has been measured with signal radiation through the substrate; see the notations with arrows in Figure 4. The corresponding curve of the CEB response is demonstrated in green with the main maximum at about 170 GHz. After the check that this sample is working and has a response, it has been bonded in another sample holder and in this case the radiation from the antenna side has been supplied. The corresponding curve of the CEB response is shown in red. In this case, one can observe the rather narrow bandwidth of the AFC in spite of the used array with bow-tie antennas with the main frequency around 210 GHz as planned, while the response is slightly smaller than in the case of radiation through the substrate. We, therefore, demonstrate the feasibility of the presented approach for the low-noise

characterization of narrow-band receiving systems with Cold-Electron Bolometers using samples intended for various frequency and power ranges.

#### 4. Conclusions

The investigation of THz properties of 50  $\mu\text{m}$  long YBCO bicrystal junctions has been performed. The oscillator chip consists of several YBCO structures integrated with the modified dipole antennas intended for various frequency ranges. For preliminary measurements of frequency response of YBCO oscillators, an array of CEBs with broadband dipole antennas was used. After characterizing the oscillators themselves, they were used to study resonant narrow-band systems based on Cold-Electron Bolometers: single detecting cells with double-folded slot antennas for 75 and 270 GHz and an array with multiple bow-tie antennas for 210 GHz, considered as a prototype of antenna for the LSPE mission.

**Author Contributions:** Conceptualization, L.S.R., I.V.R., A.V.G. and A.L.P.; Methodology, L.S.R., I.V.R. and A.L.P.; Formal analysis, L.S.R., A.V.C. and A.V.G.; Investigation, L.S.R., D.V.M., A.E.P., S.A.P., D.A.P., A.V.C., A.V.B., I.V.R., E.V.S. and A.V.G.; Data curation, L.S.R., D.A.P., A.V.C., A.V.B., E.V.S. and A.L.P.; Writing—original draft, L.S.R.; Writing—review and editing, D.A.P., A.V.G. and A.L.P.; Supervision, A.L.P.; Project administration, A.L.P. All authors have read and agreed to the published version of the manuscript.

**Funding:** This research was funded by the Russian Science Foundation, grant number 21-79-20227.

**Institutional Review Board Statement:** Not applicable.

**Informed Consent Statement:** Not applicable.

**Data Availability Statement:** The data that support the findings of this work are available from the corresponding author upon reasonable request.

**Acknowledgments:** The CEB samples were fabricated in the Chalmers Nanotechnology Centre. The YBCO JJ sample fabrication and SEM images acquisition were performed using the facilities of the Common Research Centre “Physics and technology of micro- and nanostructures” of IPM RAS. The measurements and deposition of 210 GHz bow-tie dipole antennas array were performed using the facilities of the Laboratory of Superconducting Nanoelectronics of NNSTU.

**Conflicts of Interest:** The authors declare no conflict of interest. The funders had no role in the design of the study; in the collection, analyses, or interpretation of data; in the writing of the manuscript; or in the decision to publish the results.

#### References

1. Kuzmin, L. Ultimate Cold-Electron Bolometer with Strong Electrothermal Feedback. *Proc. SPIE* **2004**, *5498*, 349.
2. Kuzmin, L. Story of the Invention of a Cold-Electron Bolometer. Available online: <https://astronomycommunity.nature.com/posts/53529-story-of-the-invention-of-a-cold-electron-bolometer> (accessed on 19 September 2019).
3. Brien, T.L.R.; Ade, P.A.R.; Barry, P.S.; Dunscombe, C.J.; Leadley, D.R.; Morozov, D.V.; Myronov, M.; Parker, E.H.C.; Prest, M.J.; Prunnila, M.; et al. Optical Response of Strained- and Unstrained-Silicon Cold-Electron Bolometers. *J. Low Temp. Phys.* **2016**, *184*, 231. [[CrossRef](#)]
4. Gordeeva, A.V.; Zbrozhek, V.O.; Pankratov, A.L.; Revin, L.S.; Shamporov, V.A.; Gunbina, A.A.; Kuzmin, L.S. Observation of photon noise by cold-electron bolometers. *Appl. Phys. Lett.* **2017**, *110*, 162603. [[CrossRef](#)]
5. Kuzmin, L.S.; Pankratov, A.L.; Gordeeva, A.V.; Zbrozhek, V.O.; Shamporov, V.A.; Revin, L.S.; Blagodatkin, A.V.; Masi, S.; de Bernardis, P. Photon-noise-limited cold-electron bolometer based on strong electron self-cooling for high-performance cosmology missions. *Comm. Phys.* **2019**, *2*, 104. [[CrossRef](#)]
6. Anghel, D.V.; Kuzmin, L.S. Cold-Electron Bolometer as a 1-cm-Wavelength Photon Counter. *Phys. Rev. Appl.* **2020**, *13*, 024028. [[CrossRef](#)]
7. Brien, T.L.R.; Ade, P.A.R.; Barry, P.S.; Dunscombe, C.J.; Leadley, D.R.; Morozov, D.V.; Myronov, M.; Parker, E.H.C.; Prest, M.J.; Prunnila, M.; et al. A Strained Silicon Cold Electron Bolometer using Schottky Contacts. *Appl. Phys. Lett.* **2014**, *105*, 043509. [[CrossRef](#)]
8. Mukhin, A.S.; Gordeeva, A.V.; Revin, L.S.; Abashin, A.E.; Shishov, A.A.; Pankratov, A.L.; Mahashabde, S.; Kuzmin, L.S. Sensitivity and Noise of Cold-Electron Bolometer Arrays. *Radiophys. Quant. Electron.* **2017**, *59*, 754. [[CrossRef](#)]
9. Tarasov, M.A.; Kuzmin, L.S.; Edelman, V.S.; Mahashabde, S.; de Bernardis, P. Optical Response of a Cold-Electron Bolometer Array Integrated in a 345-GHz Cross-Slot Antenna. *IEEE Trans. Appl. Supercond.* **2011**, *21*, 3635. [[CrossRef](#)]

10. Matrozova, E.A.; Pankratov, A.L.; Gordeeva, A.V.; Chiginev, A.V.; Kuzmin, L.S. Absorption and cross-talk in a multipixel receiving system with cold-electron bolometers. *Supercond. Sci. Technol.* **2019**, *32*, 084001. [[CrossRef](#)]
11. Zhang, Y.M. Dynamics and Applications of Long Josephson Junctions. Ph.D. Thesis, Chalmers University of Technology, Göteborg, Sweden, 1993; ISBN 91-7032-888-9.
12. Winkler, D.; Zhang, Y.M.; Nilsson, P.A.; Stepantsov, E.A.; Claeson, T. Electromagnetic Properties at the Grain Boundary Interface of a  $\text{YBa}_2\text{Cu}_3\text{O}_7$  Bicrystal Josephson Junction. *Phys. Rev. Lett.* **1994**, *72*, 1260. [[CrossRef](#)] [[PubMed](#)]
13. Kunkel, G.; Bode, M.; Wang, F.; Faley, M.I.; Siegel, M.; Zander, W.; Schubert, J.; Poppe, U.; Braginski, A.I. Comparison of Josephson radiation properties of different  $\text{YBa}_2\text{Cu}_3\text{O}_7$  thin film junctions. *Proc. SPIE-Int. Soc. Opt. Eng.* **1994**, *2160*, 33.
14. Zhang, Y.M.; Winkler, D.; Nilsson, P.-A.; Claeson, T. Josephson flux-flow resonances in overdamped long  $\text{YBa}_2\text{Cu}_3\text{O}_7$  grain-boundary junctions. *Phys. Rev. B* **1995**, *51*, 8684. [[CrossRef](#)] [[PubMed](#)]
15. Askerzade, I.; Bozbey, A.; Canturk, M. *Modern Aspects of Josephson Dynamics and Superconductivity Electronics*; Springer: Berlin/Heidelberg, Germany, 2017; 211p.
16. Masterov, D.V.; Parafin, A.E.; Revin, L.S.; Chiginev, A.V.; Skorokhodov, E.V.; Yunin, P.A.; Pankratov, A.L.  $\text{YBa}_2\text{Cu}_3\text{O}_{7-\delta}$  long Josephson junctions on bicrystal  $\text{Zr}_{1-x}\text{Y}_x\text{O}_2$  substrates fabricated by preliminary topology masks. *Supercond. Sci. Technol.* **2017**, *30*, 025007. [[CrossRef](#)]
17. Revin, L.S.; Pankratov, A.L.; Masterov, D.V.; Parafin, A.E.; Pavlov, S.A.; Chiginev, A.V.; Skorokhodov, E.V. Features of Long YBCO Josephson Junctions Fabricated by Preliminary Topology Mask. *IEEE Trans. Appl. Supercond.* **2018**, *28*, 1100505. [[CrossRef](#)]
18. Chesca, B.; John, D.; Mellor, C. Amplification of electromagnetic waves excited by a chain of propagating magnetic vortices in  $\text{YBa}_2\text{Cu}_3\text{O}_{7-\delta}$  Josephson-junction arrays at 77 K and above. *Supercond. Sci. Technol.* **2014**, *27*, 085015. [[CrossRef](#)]
19. Chesca, B.; John, D.; Gaifullin, M.; Cox, J.; Murphy, A.; Savel'ev, S.; Mellor, C.J. Magnetic flux quantum periodicity of the frequency of the on-chip detectable electromagnetic radiation from superconducting flux-flow-oscillators. *Appl. Phys. Lett.* **2020**, *117*, 142601. [[CrossRef](#)]
20. Shaikhaidarov, R.; Antonov, V.N.; Casey, A.; Kalaboukhov, A.; Kubatkin, S.; Harada, Y.; Onomitsu, K.; Tzalenchuk, A.; Sobolev, A. Detection of Coherent Terahertz Radiation from a High-Temperature Superconductor Josephson Junction by a Semiconductor Quantum-Dot Detector. *Phys. Rev. Appl.* **2016**, *5*, 024010. [[CrossRef](#)]
21. Tarasov, M.; Kuzmin, L.; Stepantsov, E.; Kidiyarova-Shevchenko, A. Quasioptical Terahertz Spectrometer Based on a Josephson Oscillator and a Cold Electron Nanobolometer. In *Nanoscale Devices—Fundamentals and Applications*, NATO Science Series; Gross, R., Sidorenko, A., Tagirov, L., Eds.; Springer: Dordrecht, The Netherlands, 2006; Volume 233, pp. 325–335.
22. Stepantsov, E.; Tarasov, M.; Kalaboukhov, A.; Kuzmin, L.; Claeson, T. THz Josephson properties of grain boundary  $\text{YBaCuO}$  junctions on symmetric, tilted bicrystal sapphire substrates. *J. Appl. Phys.* **2004**, *96*, 3357. [[CrossRef](#)]
23. Revin, L.; Pankratov, A.; Gordeeva, A.; Masterov, D.; Parafin, A.; Zbrozhek, V.; Kuzmin, L. Response of a Cold-Electron Bolometer on THz Radiation from a Long  $\text{YBa}_2\text{Cu}_3\text{O}_{7-\delta}$  Bicrystal Josephson Junction. *Appl. Sci.* **2020**, *10*, 7667. [[CrossRef](#)]
24. Revin, L.; Pimanov, D.A.; Blagodatkin, A.V.; Gordeeva, A.V.; Pankratov, A.L.; Chiginev, A.V.; Rakut', I.V.; Zbrozhek, V.O.; Kuzmin, L.S.; Masi, S.; et al. Spectral Characteristics of the Double-Folded Slot Antennas with Cold-Electron Bolometers for the 220/240 GHz Channels of the LSPE Instrument. *Appl. Sci.* **2021**, *11*, 10746. [[CrossRef](#)]
25. Tarasov, M.; Stepantsov, E.; Lindstrom, T.; Lohmus, A.; Ivanov, Z. Submillimeter-wave quasioptical integrated tester based on bicrystal Josephson junctions. *Phys. C Supercond. Appl.* **2002**, *372–376*, 347. [[CrossRef](#)]
26. Kuzmin, L.S.; Sobolev, A.S.; Beiranvand, B. Wideband Double-Polarized Array of Cold-Electron Bolometers for OLIMPO Balloon Telescope. *IEEE Trans. Antennas Propag.* **2020**, *69*, 1427. [[CrossRef](#)]
27. Gordeeva, A.V.; Pankratov, A.L.; Pugach, N.G.; Vasenko, A.S.; Zbrozhek, V.O.; Blagodatkin, A.V.; Pimanov, D.A.; Kuzmin, L.S. Record electron self-cooling in cold-electron bolometers with a hybrid superconductor-ferromagnetic nanoabsorber and traps. *Sci. Rep.* **2020**, *10*, 21961. [[CrossRef](#)] [[PubMed](#)]
28. Salatino, M.; de Bernardis, P.; Kuzmin, L.S.; Mahashabde, S.; Masi, S. Sensitivity to cosmic rays of cold electron bolometers for space applications. *J. Low Temp. Phys.* **2014**, *176*, 323. [[CrossRef](#)]
29. O'Brient, R.; Ade, P.; Arnold, K.; Edwards, J.; Engargiola, G.; Holzapfel, W.L.; Lee, A.T.; Myers, M.J.; Quealy, E.; Rebeiz, G.; et al. A dual-polarized broadband planar antenna and channelizing filter bank for millimeter wavelengths. *Appl. Phys. Lett.* **2013**, *102*, 063506. [[CrossRef](#)]
30. Kuzmin, L.S.; Blagodatkin, A.V.; Mukhin, A.S.; Pimanov, D.A.; Zbrozhek, V.O.; Gordeeva, A.V.; Pankratov, A.L.; Chiginev, A.V. Multichroic seashell antenna with internal filters by resonant slots and cold-electron bolometers. *Supercond. Sci. Technol.* **2019**, *32*, 035009. [[CrossRef](#)]
31. Gundareva, I.; Pavlovskiy, V.; Divin, Y. High- $T_c$  Josephson Junctions as Quasiclassical THz Detectors. *IEEE Trans. Appl. Supercond.* **2018**, *28*, 1800105. [[CrossRef](#)]
32. Kuzmin, L.S.; Chiginev, A.V.; Matrozova, E.A.; Sobolev, A.S. Multifrequency Seashell Slot Antenna With Cold-Electron Bolometers for Cosmology Space Missions. *IEEE Trans. Appl. Supercond.* **2016**, *26*, 2300206. [[CrossRef](#)]
33. Lamagna, L.; Addamo, G.; Ade, P.A.R.; Baccigalupi, C.; Baldini, A.M.; Battaglia, P.M.; Battistelli, E.; Baù, A.; Bersanelli, M.; Biasotti, M.; et al. Progress Report on the Large-Scale Polarization Explorer. *Low Temp. Phys.* **2020**, *200*, 374–383. [[CrossRef](#)]
34. Chiginev, A.V.; Blagodatkin, A.V.; Pimanov, D.A.; Matrozova, E.A.; Gordeeva, A.V.; Pankratov, A.L.; Kuzmin, L.S. Numerical modeling of a multi-frequency receiving system based on an array of dipole antennas for LSPE-SWIPE. *Beilstein J. Nanotechnol.* **2022**, *13*, 865–872. [[CrossRef](#)]